NASA CONTRACTOR REPORT

NASA CR-2310

NASA CR-2310

AN EFFICIENT TECHNIQUE FOR DETERMINING APPARENT TEMPERATURE DISTRIBUTIONS FROM ANTENNA TEMPERATURE MEASUREMENTS

by John P. Claassen and A. K. Fung

Prepared by
THE UNIVERSITY OF KANSAS CENTER FOR RESEARCH, INC.
Lawrence, Kans. 66044
for Langley Research Center

NATIONAL AERONAUTICS AND SPACE ADMINISTRATION • WASHINGTON, D. C. • SEPTEMBER 1973

1. Report No.	2. Government Accession No.	3. Recipient's Catalog No.
NASA CR-2310		

4. Title and Subtitle	5. Report Date
An Efficient Technique for Determining Apparent Temperature Distributions from Antenna Temperature Measurements	September 1973
	6. Performing Organization Code

7. Author(s)	8. Performing Organization Report No.
John P. Claassen and A. K. Fung	TR 186-8
	10. Work Unit No.

9. Performing Organization Name and Address	11. Contract or Grant No.
The University of Kansas Center for Research, Inc. 2291 Irving Hill Road - Campus West Lawrence, Kansas 66044	NAS 1-10048
	13. Type of Report and Period Covered
12. Sponsoring Agency Name and Address	Contractor Report
National Aeronautics and Space Administration Washington, D. C. 20546	14. Sponsoring Agency Code

15. Supplementary Notes

This is a topical report.

16. Abstract

A method by which the apparent microwave temperature characteristic of a flat scene is estimated from dual polarized measurements is derived and interpreted. Approximate linear relationships between antenna and apparent temperatures are established by weighting emission components in spherical bands under the assumption that the surface is isotropic. The weighting factors are formed by integrating the antenna pattern functions over these bands. The vector aspect of the formulation is retained to account for the difference between the definition of the antenna polarizations and the polarizations of the emitted fields. The method is largely applicable to the measurement of smooth temperature distributions by an antenna having good spatial resolution of the distributions and is considered efficient for inverting large volumes of measurements.

Sample cases are presented and the implications of these cases on remote radiometer observations are discussed. It is shown that cross-coupling occurs between the polarizations of the emitted fields and the polarizations of the antenna. For this reason and because practical antennas have cross-polarized patterns associated with them, it is necessary to conduct measurements at both horizontal and vertical polarizations to realize the inversion. It is also made evident that thorough inversions require that the apparent temperatures be sampled at a sufficient number of points between nadir and zenith.

17. Key Words (Suggested by Author(s))	18. Distribution Statement
Apparent microwave temperature Antenna temperature Inversion	Unclassified - unlimited

19. Security Classif. (of this report)	20. Security Classif. (of this page)	21. No. of Pages	22. Price*
Unclassified	Unclassified	33	Domestic, $3.00 Foreign, $5.50

*For sale by the National Technical Information Service, Springfield, Virginia 22151

INTRODUCTION

A. Motivation

In the discipline of microwave radiometry it is often important to determine the complete emission characteristic of a flat scene. The emission characteristic is commonly estimated from a set of antenna temperature measurements conducted at a number of observation angles from a remote observation point. It is well known that good estimates of the brightness temperature distribution require that the measurements be compensated for (1) antenna pattern weighting of the distributions, and (2) direct and reflected atmospheric emission contributions. Compensation for antenna pattern weighting yields the apparent temperature distribution about the point of observation. Extraction of the direct and reflected contributions from the apparent temperature distribution then yields the brightness temperature characteristic of the scene. Corrections of either type represent rather formidable tasks both in the implementation of the experiment and in the reduction of the data. The precision inherent in the radiometer can, however, only be realized in estimating the temperature distribution when thorough and efficient methods for handling both types of corrections are employed.

Various methods to estimate the apparent temperature have been used. In some instances it was common practice to use the antenna temperature as an estimate of the apparent temperature (and sometimes mistakenly as the brightness temperature). However, Peake et al.[1], using a recursive inversion technique, have vividly illustrated the difference between the antenna temperature and the apparent temperature. Fourier transform techniques have been reported [2,3,4], largely by members of the radio astronomy community. In these methods repeated and sometimes lengthy numerical double integrations are required to estimate the apparent temperature for each scene. They are, as a consequence, inefficient for handling large volumes of data as often collected by those engaged in remote sensing programs.

An efficient as well as comprehensive method for estimating the apparent temperature distribution has been derived for isotropic scenes. The antenna weights on the vertically and horizontally polarized emission components are formed by a linear mathematical model which when invertible yields the apparent temperature distribution. It is shown that radiometric observations at both polarizations are required at a number of angles between nadir and zenith to recover the apparent temperature distributions.

B. Background

The antenna temperature inversion problem is mathematically akin to a host of physical problems in which a function f(x) is to be inferred from measurements g(y) taken by a linear system where the measurements are related to f(x) by a Fredholm equation of the first kind

$$g(y) = \int_a^b K(x,y)\, f(x)\, dx \qquad (1)$$

In this particular application f(x) is to be regarded as the apparent temperature distribution, the kernel K(x,y) as the antenna power pattern and g(y) as the antenna temperature.

Various inversion techniques for (1) have been proposed. When main beam smoothing is the dominant effect, a "desmoothing" technique as suggested by Bracewell [5] can be employed. In the general inversion problem, more than the main beam will play an important role, however. When the functional form of f(x) is known on an a priori basis, except for a set of unknown parameters, very often the optimum member of a family can be determined by comparing the measurements in the least squares sense with an algebraic representation of (1). This type of approach is often suggested for sky temperature measurements [6]. However, for terrestial and ocean scenes the apparent temperature distribution is not known on an a priori basis. Furthermore, any technique suggested for sky temperature measurements would not be appropriate for the general case since emissions from the atmosphere are usually considered independent of polarization. An iterative technique similar to to Picard's process of successive approximations [7] has been reported [1,8]. Sometimes called the boot-strap technique, this method uses the measured g(x) as the first estimate of f(x). When the measurement is subject to noise, convergence of the iterative technique is not assured in practice [8], [9]. A Fourier inversion technique based on interferometric measurements is employed by the radio astronomer. The technique, however, is restricted to sources of small angular extent [3], [10]. Here a method is sought for expansive flat scenes such as the ocean.

C. Approach

A matrix formulation of the integral equation relating the apparent temperature to the antenna temperature is employed here. Pictorially, the antenna is located at the center of a spherical coordinate system and is observing a cylindrically symmetric temperature distribution* on a sphere. The cylindrical symmetry applies to the upper and lower half spaces separately. The temperature distribution, however, is approximated by spherical bands at constant temperature as illustrated in Figure 1. When the antenna "points" at the midpoint of one of these bands, the antenna temperature is considered a linear sum of the antenna weights on each band. The antenna weights for observations on all bands form the modeling matrix. This approach must therefore assume that the apparent temperature distributions are smooth functions so that they can be approximated by a constant over each band.** The antenna main beam is considered sufficiently narrow to spatially resolve temperature differences between adjacent bands.

Particular attention is given to generalized descriptions of the antenna patterns. Here, it is assumed that the patterns were measured from an azimuth-over-elevation mount so as to preserve the notion of polarizations as defined in a spherical coordinate system. Each polarized pattern is considered to be accompanied by a cross-polarized pattern of generally smaller intensity. The cross polarized component is assumed to be coupled in phase with the polarized component. The antenna polarizations (somewhat surprisingly) do not in general coincide with the surface polarizations.*** The formulation as a consequence distinguishes the two carefully and therefore accounts for cross-coupling between antenna and surface polarizations.

In a matrix formulation of this type the user must be keenly aware that under some circumstances the linear model can become ill-conditioned [11], particularly when the model is developed at the limit of the antenna resolution. In some circumstances an ill-conditioned model can be salvaged by amending the formulation with numerical filtering [12].

---

* Not a necessary assumption, although once discarded the formulation becomes unwieldy as well as the measurements.

** Experience has shown that several bands can violate this assumption without adversely affecting the inversion estimates on the other bands.

***This peculiarity was made clear by W. H. Peake of Ohio State University in a private communication.

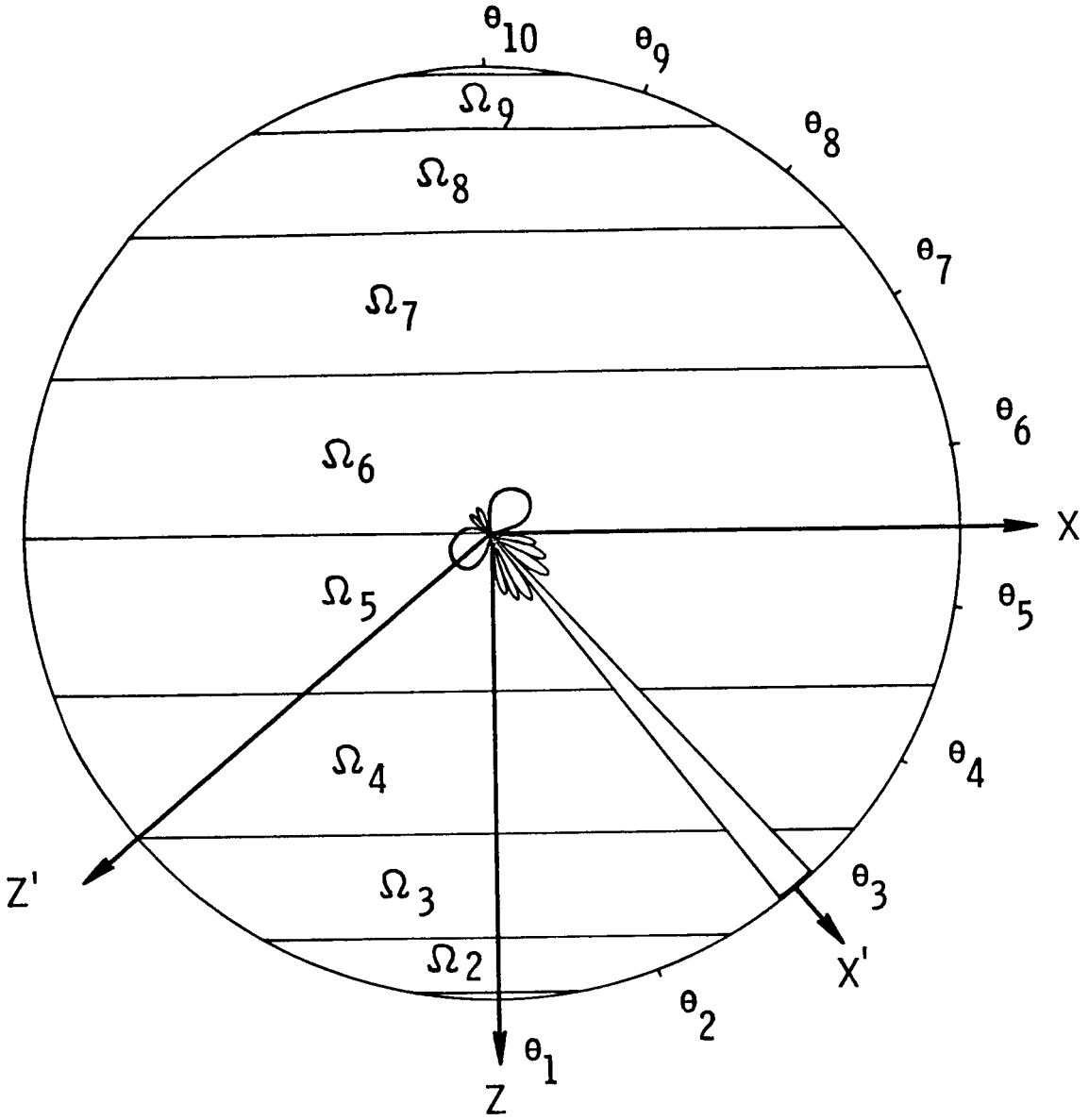

FIGURE 1. AN ILLUSTRATION DEPICTING THE TECHNIQUE BEHIND THE INVERSION MODEL

THEORETICAL DEVELOPMENT

A. Description of the Antenna Pattern

A dual polarized antenna is located at the origin of a primed coordinate system (see Figure 2). The boresight is directed along the positive x' axis. When the v-port is energized and the h port is terminated, the vertically polarized pattern is generated. The E plane coincides with x'z' plane. Similarly, when the h port is energized and the v port terminated, the horizontally polarized pattern is generated. The x'y' plane coincides with its E plane. Each polarized pattern is assumed to be accompanied by a cross-polarized pattern. In general, the polarized field is coupled in phase to the cross-polarized field when the antenna is regarded as a transmitter. The resultant field is consequently elliptically polarized. By the reciprocity theorem it is understood that the reception property has a similar polarization character. The phase coupling, however, must be regarded as the complex conjugate of that when the antenna is viewed as a transmitter. For the polarization discriminant antenna, the effect is weak since the cross polarized pattern is assumed to have considerably smaller power content. However, a general viewpoint will be retained since the radiometer antenna receives partially polarized fields [13]. The orientations of the antenna polarizations are defined in terms of spherical unit vectors as illustrated in Figure 2.

In view of the elliptically polarized character of the antenna, the reception property will be described in terms of a vector complex effective height. For the p^{th} (p = v or h) port the effective height is denoted by

$$\underset{\sim}{\mathcal{R}}_p = \frac{\lambda}{\sqrt{4\pi}} \sqrt{G_p(\theta', \phi')} \quad \underset{\sim}{\rho}_p(\theta', \phi') \qquad (2)$$

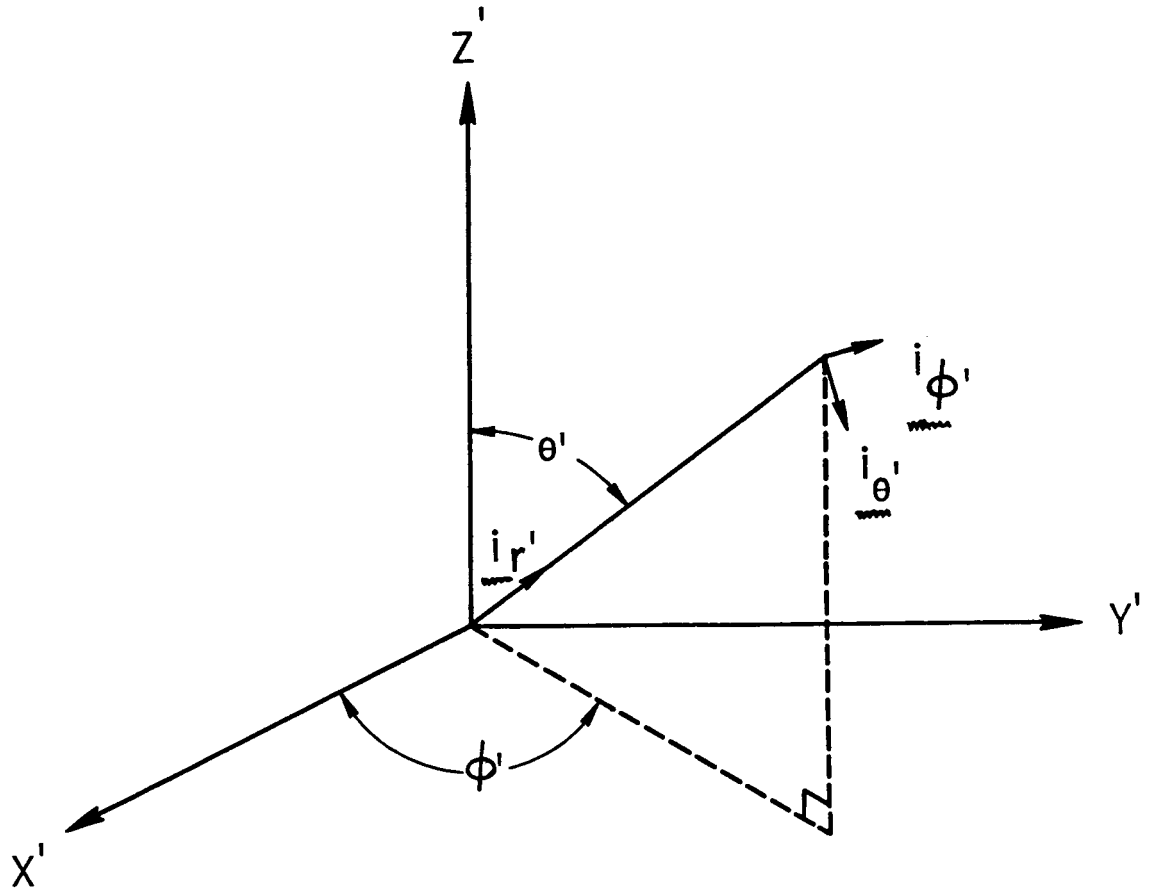

HORIZONTAL POLARIZATION

$$i_{\phi'} = i_{r'} \times i_{\theta'}$$

VERTICAL POLARIZATION

$$i_{\theta'} = i_{\phi'} \times i_{r'}$$

FIGURE 2. GEOMETRY FOR PATTERN MEASUREMENTS

where

λ = mean operating wavelength

$G_p(\theta'\phi')$ = elliptically polarized power gain

$$\rho_p(\theta', \phi') = \gamma_p \hat{i}_{\theta'} + \delta_p \hat{i}_{\phi'} \qquad (3)$$

R_p may be identified with the reception factor defined by Kales [14]. In expression (3) γ_p and δ_p are complex functions of θ' and ϕ' and denote the relative sensitivity to a polarized field and a cross polarized field. The components of $|R_p|^2$ are related to the typically measured normalized patterns g_{p1} and g_{p2} by the following expressions

$$g_{p1}(\theta', \phi') = \frac{\lambda_p}{4\pi} \frac{G_p(\theta', \phi') |\gamma_p|^2}{\eta_p} \qquad (4)$$

$$g_{p2}(\theta', \phi') = \frac{\lambda_p}{4\pi} \frac{G_p(\theta', \phi') |\delta_p|^2}{\eta_p} \qquad (5)$$

where

g_{v1} (g_{h2}) = vertically (horizontally) polarized pattern

g_{v2} (g_{h1}) = cross polarized pattern associated with g_{v1} (g_{h2})

$$\Lambda_p = \iint_{4\pi} (g_{p1} + g_{p2}) \, d\Omega \qquad (6)$$

η_p = radiation efficiency

In the following development it will be convenient to consider the radiation efficiency factor as unity and to incorporate its effect in the radiometer transfer function. The antenna is therefore idealized.

The relative phase between the polarized and cross polarized fields must be measured to establish the phasor characters of γ_p and δ_p. To understand the nature of ρ_p it is helpful to write it in the coordinate frame coinciding with the principal axes of the polarization ellipse. Let ι_1 and ι_2 denote orthogonal unit vectors coinciding with the principal axes for a particular look direction. Then

$$\underset{\sim}{\rho}_p = \cos\chi \, \underset{\sim}{i}_1 + j \sin\chi \, \underset{\sim}{i}_2 \qquad (7)$$

where $|\tan\chi|$ is the axial ratio. Now let ξ denote the angle of rotation between the principal axes and the antenna polarization vectors as illustrated in Figure 3. Then

$$\underset{\sim}{\rho}_p = (\cos\chi\cos\xi - j\sin\chi\sin\xi)\,\underset{\sim}{i}_{\theta'} + (\cos\chi\sin\xi + j\sin\chi\cos\xi)\,\underset{\sim}{i}_{\phi'} \qquad (8)$$

The terms within the brackets are identified as γ_p and δ_p, respectively, for this particular look direction.

B. Geometry of the Measurement Coordinate System

The above described antenna is now positioned at a height H above a "flat" scene whose emission characteristic is to be measured. The antenna is considered to be located in an absorbing/emitting atmosphere. The geometry of the scene is

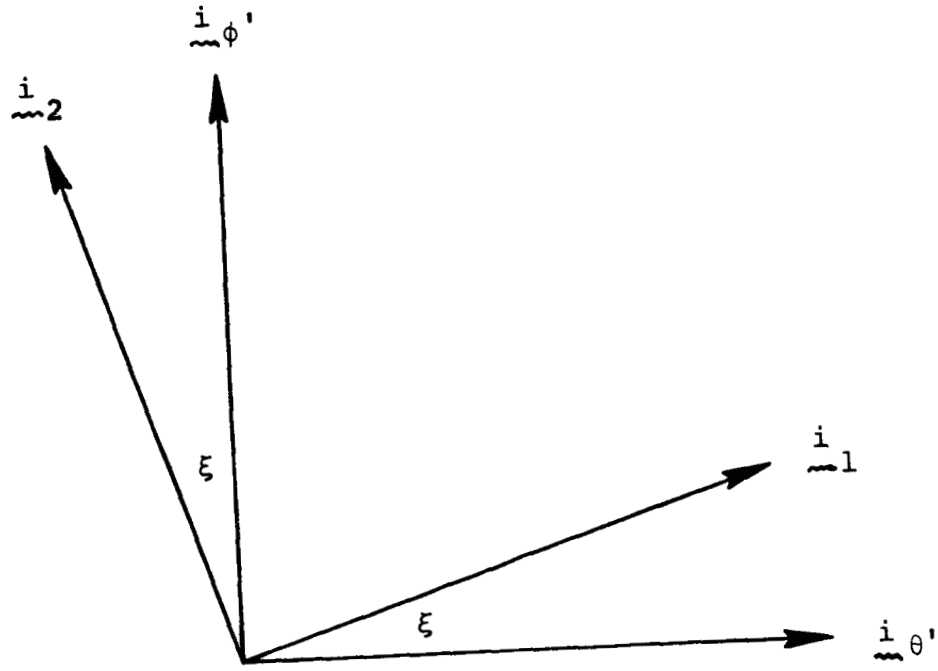

FIGURE 3. PRINCIPAL POLARIZATION AXES RELATIVE TO THE ANTENNA POLARIZATION VECTORS

described in terms of an unprimed coordinate system whose z axis points downward (see Figure 4). The antenna scans in the xz plane from nadir to zenith. In this plane the look direction θ_o is defined as the angle between the boresight axis x' and the z axis. The angle θ_o also describes the rotation about an axis common to the antenna and scene coordinate frames.

C. Development of the Inversion Model

The antenna observes an angular distribution of non-coherent sources represented by the electric field intensity

$$\underset{\sim}{E}(\theta, t) = E_\theta \, \underset{\sim}{i}_\theta + E_\phi \, \underset{\sim}{i}_\phi \qquad (9)$$

where E_θ and E_ϕ are complex functions of θ and t. Since the bandwidth of receiver B is considered much smaller than the frequency of observation, both E_θ and E_ϕ may be considered quasi-monochromatic in character [13]. The emission components of the surface below or, for that matter, of a sphere surrounding the observation point are described in the unprimed coordinate system. The emitted polarizations are so chosen to agree with the standard definitions for the polarizations of a planar surface (see Figure 4). For an observation in the θ_o direction the average power available at the p^{th} port of the antenna is therefore given by

$$P_p(\theta_o) = \frac{1}{4\pi\eta_o} \iint_{4\pi} \langle | \underset{\sim}{E} \cdot \underset{\sim}{R}_p |^2 \rangle \, d\Omega \qquad p = v \text{ or } h \qquad (10)$$

where

$$\underset{\sim}{E} \cdot \underset{\sim}{R}_p = \frac{\lambda}{\sqrt{4\pi}} \sqrt{G_p(\theta', \phi')} \left[E_\theta \, \underset{\sim}{i}_\theta \cdot (\gamma_p \, \underset{\sim}{i}_{\theta'} + \delta \, \underset{\sim}{i}_{\phi'}) + E_\phi \, \underset{\sim}{i}_\phi \, (\gamma_p \, \underset{\sim}{i}_{\theta'} + \delta_p \, \underset{\sim}{i}_{\phi'}) \right] \qquad (11)$$

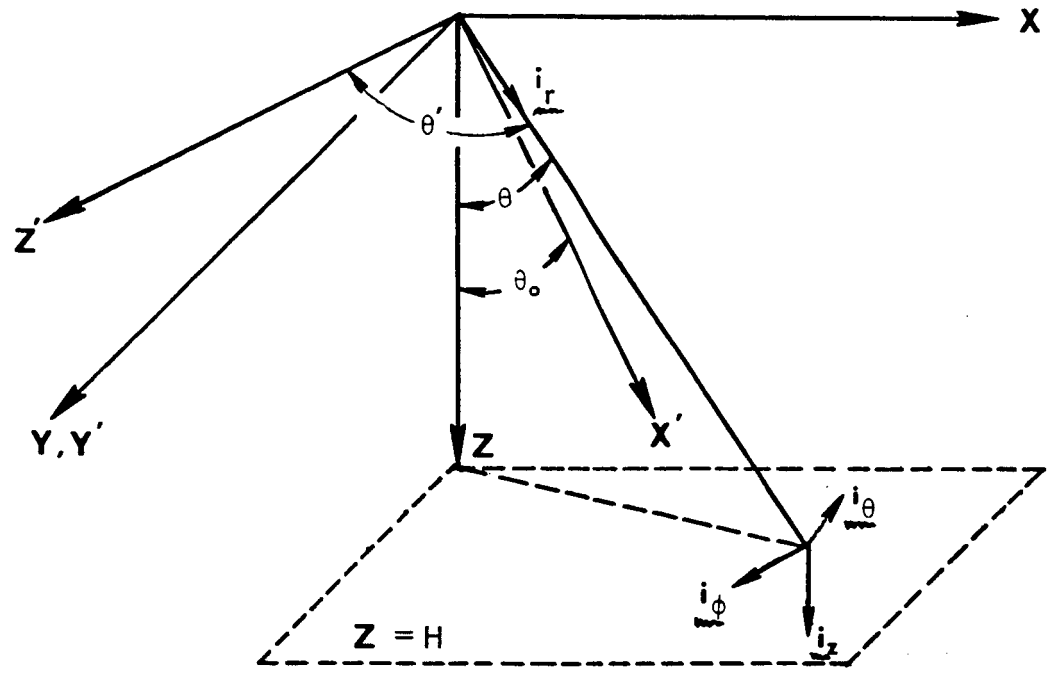

HORIZONTAL POLARIZATION

$$\underset{\sim}{i}_\phi = \frac{\underset{\sim}{i}_z \times \underset{\sim}{i}_r}{|\underset{\sim}{i}_z \times \underset{\sim}{i}_r|}$$

VERTICAL POLARIZATION

$$\underset{\sim}{i}_\theta = \underset{\sim}{i}_\phi \times \underset{\sim}{i}_r$$

FIGURE 4. GEOMETRY OF THE OBSERVATION COORDINATE SYSTEM RELATIVE TO THAT OF THE ANTENNA COORDINATE SYSTEM

and

η_o = intrinsic impedance

The integrand of (10) when expanded, contains a number of terms involving auto-correlations and cross-correlations of the type $\langle E_\theta E_\theta^* \rangle$ and $\langle E_\phi E_\theta^* \rangle$, respectively. For a flat scene it is easily shown that the cross-correlation terms vanish when the emissions are formulated in terms of the vertically $\underset{\sim}{\iota}_\theta$ and horizontally $\underset{\sim}{\iota}_\phi$ polarized states. On the otherhand, the auto-correlation terms are related to the apparent temperatures T_θ and T_ϕ by the expressions [15]

$$\frac{\langle |E_\theta|^2 \rangle}{\eta_o} = \frac{4\pi k T_\theta B}{\lambda^2} \tag{12}$$

and

$$\frac{\langle |E_\phi|^2 \rangle}{\eta_o} = \frac{4\pi k T_\phi B}{\lambda^2} \tag{13}$$

Here k is Boltzmann's constant. T_θ is the vertically polarized contribution; whereas T_ϕ is the horizontally polarized contribution.

The vector inner products generated in the integrand may be reduced to trigonometric expressions. It is noted that the orthogonal pairs $(\underset{\sim}{\iota}_\theta, \underset{\sim}{\iota}_\phi)$ and $(\underset{\sim}{\iota}_{\theta'}, \underset{\sim}{\iota}_{\phi'})$ are mutually orthogonal to a line of sight vector $\underset{\sim}{\iota}_r$. The orthogonal pairs are therefore related by a simple rotation as illustrated in Figure 5. It follows that

$$\begin{aligned} \underset{\sim}{i}_\theta \cdot \underset{\sim}{i}_{\theta'} &= \underset{\sim}{i}_\phi \cdot \underset{\sim}{i}_{\phi'} = \cos\psi \\ \underset{\sim}{i}_\theta \cdot \underset{\sim}{i}_{\phi'} &= -\underset{\sim}{i}_\phi \cdot \underset{\sim}{i}_{\theta'} = \sin\psi \end{aligned} \tag{14}$$

When the received power $P_p(\theta_o)$ is translated into an equivalent antenna temperature, Equation (10) in view of the above observations and equations (4) and (5), can be written as

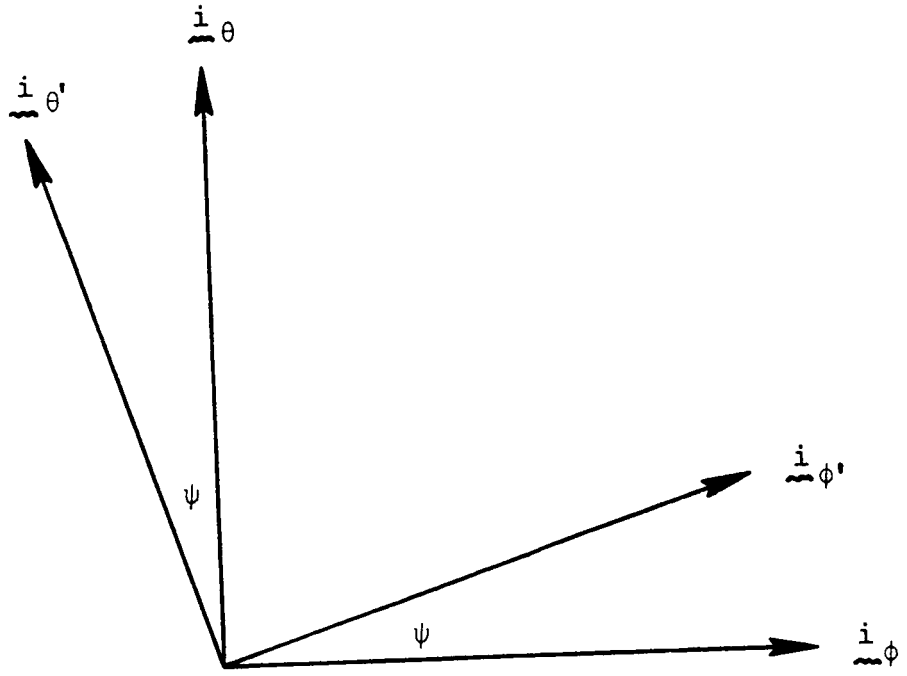

FIGURE 5. RELATIONSHIP BETWEEN ANTENNA AND SURFACE POLARIZATIONS

$$T_p(\theta_o) = \frac{1}{\Lambda_p} \iint \left\{ T_\theta \left[g_{p1} \cos^2\psi + g_{p2} \sin^2\psi \right] + T_\phi \left(g_{p1} \sin^2\psi + g_{p2} \cos^2\psi \right) + \left[T_\theta - T_\phi \right] \sqrt{g_{p1} g_{p2}} \cos\beta_p \sin 2\psi \right\} d\Omega \tag{15}$$

where

$$\beta_p = \tan^{-1} \left[\frac{\mathcal{I}m(\gamma_p \delta_p^*)}{\mathcal{R}e(\gamma_p \delta_p^*)} \right] \tag{16}$$

Suppose the temperature distributions are sampled at both antenna polarizations over the interval $0 \leqslant \theta_o \leqslant \pi$. Denote the observation angles as $0 \leqslant \theta_1 < \theta_2 < \ldots < \theta_n \leqslant \pi$. Under the assumption that the temperature distributions can be approximated by spherical bands at constant temperatures, the antenna temperatures at θ_k may be approximated by

$$T_v(\theta_k) = \sum_{j=1}^{n} \left[a_{kj} T_\theta(\theta_j) + b_{kj} T_\phi(\theta_j) \right] \tag{17}$$

$$T_h(\theta_k) = \sum_{j=1}^{n} \left[c_{kj} T_\theta(\theta_j) + d_{kj} T_\phi(\theta_j) \right] \tag{18}$$

where

$$a_{kj} = \frac{1}{\Lambda_v} \iint \left[g_{v1} \cos^2\psi + g_{v2} \sin^2\psi + \sqrt{g_{v1} g_{v2}} \sin 2\psi \cos\beta_v \right] d\Omega$$

$$b_{kj} = \frac{1}{\Lambda_v} \iint \left[g_{v1} \sin^2\psi + g_{v2} \cos^2\psi - \sqrt{g_{v1} g_{v2}} \sin 2\psi \cos\beta_v \right] d\Omega \tag{19}$$

$$c_{kj} = \frac{1}{\Lambda_h} \iint \left[g_{h1} \cos^2\psi + g_{h2} \sin^2\psi + \sqrt{g_{h1} g_{h2}} \sin 2\psi \cos\beta_h \right] d\Omega$$

$$d_{kj} = \frac{1}{\Lambda_h} \iint \left[g_{h1} \sin^2\psi + g_{h2} \cos^2\psi - \sqrt{g_{h1} g_{h2}} \sin 2\psi \cos\beta_h \right] d\Omega$$

$$\Omega_j = \left\{ (\theta, \phi) : \frac{\theta_{j-1} + \theta_j}{2} \le \theta \le \frac{\theta_j + \theta_{j+1}}{2} , \right.$$

$$\left. 0 \le \phi \le 2\pi , \quad 1 < j < n \right\}$$

$$\Omega_1 = \left\{ (\theta, \phi) : 0 \le \theta \le \theta_1/2 , \quad 0 \le \phi \le 2\pi \right\} \qquad (20)$$

and $$\Omega_n = \left\{ (\theta, \phi) : \frac{\pi + \theta_{n-1}}{2} \le \theta \le \pi , \; 0 \le \phi \le 2\pi \right\}$$

The integrations are to be specifically performed in the unprimed coordinate system as defined by Ω_j. As will be seen, the integrands are functions of θ_k and thereby justify the kj subscripts for the constants a, b, c and d. The density of measurements must be sufficient to justify the approximation that the apparent temperatures, T_θ and T_ϕ, are essentially constant on each spherical band Ω_j.

The above system of equations (11) and (12) can be written in a compact form with partitioned matrices

$$\begin{bmatrix} T_v \\ T_h \end{bmatrix} = \begin{bmatrix} A & B \\ C & D \end{bmatrix} \begin{bmatrix} T_\theta \\ T_\phi \end{bmatrix} \qquad (21)$$

where

$$\begin{bmatrix} T_v \\ T_h \end{bmatrix} = \begin{bmatrix} T_v(\theta_1) \\ T_v(\theta_2) \\ \vdots \\ T_v(\theta_n) \\ T_h(\theta_1) \\ T_h(\theta_2) \\ \vdots \\ T_h(\theta_n) \end{bmatrix} , \qquad \begin{bmatrix} T_\theta \\ T_\phi \end{bmatrix} = \begin{bmatrix} T_\theta(\theta_1) \\ T_\theta(\theta_2) \\ \vdots \\ T_\theta(\theta_n) \\ T_\phi(\theta_1) \\ T_\phi(\theta_2) \\ \vdots \\ T_\phi(\theta_n) \end{bmatrix} \qquad (22)$$

and $$(A)_{kj} = a_{kj} \qquad (B)_{kj} = b_{kj} \qquad (C)_{kj} = c_{kj} \qquad (D)_{kj} = d_{kj} \qquad (23)$$

The matrix [A,B] contains the antenna weights for the vertically polarized observations and [C, D] contains the antenna weights for the horizontally polarized observations. The B matrix denotes the horizontally polarized contributions to the vertically polarized observations, whereas the C matrix denotes the vertically polarized contributions to the horizontally polarized observations. When the modelling matrix is invertible, the apparent temperature distribution is approximated by

$$\begin{bmatrix} T_\theta \\ T_\phi \end{bmatrix} = \begin{bmatrix} A & B \\ C & D \end{bmatrix}^{-1} \begin{bmatrix} T_v \\ T_h \end{bmatrix} \tag{24}$$

For symmetric and identical v and h antenna patterns the modeling matrix (21) must be simplified when observations are conducted at nadir and zenith. The first and last rows of [A B] are, in this case, identical to the first and last rows of [C D]. The isotropic assumption permits removal of the redundant rows, say those in [C D]. The corresponding antenna weights located in the first and last columns of $\begin{bmatrix} B \\ D \end{bmatrix}$, however, must be added to the first and last columns of $\begin{bmatrix} A \\ C \end{bmatrix}$, respectively. The resulting model is then expressed as

$$\begin{bmatrix} T_v \\ T_{h'} \end{bmatrix} = \begin{bmatrix} A' & B' \\ C' & D' \end{bmatrix} \begin{bmatrix} T_\theta \\ T_{\phi'} \end{bmatrix} \tag{25}$$

where primes reflect the removal of rows and columns and the summation of the indicated columns.

It is of interest to note that for a non-precipitating atmosphere the emissions coming totally from the atmosphere are polarization invariant. As a consequence the latter elements in T_θ, say $T_\theta(\theta_k)$, $T_\theta(\theta_{k+1})$ . . . , $T_\theta(\theta_n)$, are redundant with the respective latter elements in T_ϕ, say $T_\phi(\theta_k)$, $T_\phi(\theta_{k+1})$ . . ., $T_\phi(\theta_n)$. In this circumstance, the modelling matrix can be altered in either of two ways. If observations above the horizons are conducted only at one polarization, the modelling matrix may be collapsed by removing the rows associated with the deleted observations. The associative columns must be removed and added to the columns corresponding to the polarized observations which have been retained. The result is a square matrix whose inverse will estimate the apparent temperature distributions. On the otherhand, if observations at both polarizations are retained above the horizon, the original modelling matrix may be solved subject to the constraint that $T_\theta(\theta_j) = T_\phi(\theta_j)$, $j=k, k+1, \ldots, n$. In this case, all the rows are retained; however, columns k through n in $\begin{bmatrix} B \\ D \end{bmatrix}$ are removed and added to the corresponding columns of $\begin{bmatrix} A \\ B \end{bmatrix}$. The resulting rectangular system may be solved by the least squares method. It is anticipated that the latter technique will yield better temperature estimates above the horizon than the initial one.

Under the isotropic assumption either one of the above two procedures (applied to the observations above the horizon) may also be applied to the nadir observations. The latter procedure will also work for symmetric patterns.

D. Computation of the Elements in the Model

From a practical viewpoint the elements in the radiometer inversion model (21) must be evaluated numerically. Since the integrations are to be performed over spherical bands Ω_j, the arguments of the integrand functions, as a matter of convenience, must be expressed in terms of the unprimed coordinates. The transformation between the coordinate systems is clearly (see Figure 4) given by

$$\begin{pmatrix} \underset{\sim}{i}_{x'} \\ \underset{\sim}{i}_{y'} \\ \underset{\sim}{i}_{z'} \end{pmatrix} = \begin{pmatrix} \sin\theta_0 & 0 & \cos\theta_0 \\ 0 & 1 & 0 \\ -\cos\theta_0 & 0 & \sin\theta_0 \end{pmatrix} \begin{pmatrix} \underset{\sim}{i}_{x} \\ \underset{\sim}{i}_{y} \\ \underset{\sim}{i}_{z} \end{pmatrix} \tag{26}$$

Now from (14) it is recalled that

$$\cos\psi = \underset{\sim}{i}_{\phi} \cdot \underset{\sim}{i}_{\phi'} \tag{27}$$

We also have

$$\begin{aligned} \underset{\sim}{i}_{\phi} &= -\sin\phi\, \underset{\sim}{i}_{x} + \cos\phi\, \underset{\sim}{i}_{y} \\ \underset{\sim}{i}_{\phi'} &= -\sin\phi'\, \underset{\sim}{i}_{x'} + \cos\phi'\, \underset{\sim}{i}_{y'} \end{aligned} \tag{28}$$

As a consequence

$$\cos\psi = \cos\phi\cos\phi' - \sin\phi\sin\phi'\sin\theta_0 \tag{29}$$

Furthermore, to eliminate $\cos\phi'$ and $\sin\phi'$, it is noted that

$$\tan\phi' = \frac{\underset{\sim}{i}_{r} \cdot \underset{\sim}{i}_{y'}}{\underset{\sim}{i}_{r} \cdot \underset{\sim}{i}_{x'}} \tag{30}$$

or

$$\tan\phi' = \frac{\sin\theta\sin\phi}{\cos\theta\cos\theta_0 + \sin\theta\sin\theta_0\cos\phi} \tag{31}$$

where

$$\underset{\sim}{i}_{r} = \sin\theta\cos\phi\, \underset{\sim}{i}_{x} + \sin\theta\cos\phi\, \underset{\sim}{i}_{y} + \cos\theta\, \underset{\sim}{i}_{z} \tag{32}$$

has been used.

Relationships (29) and (31) resolve the Ψ and ϕ' dependence on θ and ϕ. The θ' dependence on θ and ϕ is established by

$$\cos\theta' = \underset{\sim}{i}_r \cdot \underset{\sim}{i}_z \tag{33}$$

or

$$\cos\theta' = \cos\theta \sin\theta_o - \sin\theta \cos\theta_o \cos\phi \tag{34}$$

SIMULATION RESULTS

A. Introduction

To evaluate the radiometer inversion model posed above, computer simulation studies were conducted. With an assumed set of antenna patterns and assumed apparent temperature distributions, antenna temperatures were accurately computed at ten degree intervals. These antenna temperatures were employed in a matrix inversion model based on observations at 10 degree intervals. By means of the inverse, the apparent temperature distributions were recovered and compared with the original temperature distributions. The implementation and results of these studies are described below.

B. Computation of Elements in the Model

Functional representations of the AAFE RADSCAT antenna* patterns were employed to evaluate the weighting factors (elements) in the radiometer inversion model (17) - (20). The h plane pattern at 13.9 GHz is shown in Figures 6. The polarized main beam, the first few side-lobes (partially embedded in main beam), the cross-polarized beams, and the spill-over side lobes, were all approximated with Gaussian functions. The band of side lobes around the main beam was approximated with a cylindrical cone as shown by the dashed lines in Figure 6. Since the back lobes were insignificant, they were ignored in these studies. In addition to the polarized pattern, a representation for the cross polarized pattern (not shown) was also employed.

*The AAFE RADSCAT antenna is a rear fed parabolic antenna developed under NASA Contract NAS 1-10161 by General Electric Space Division, Philadelphia, Pa.

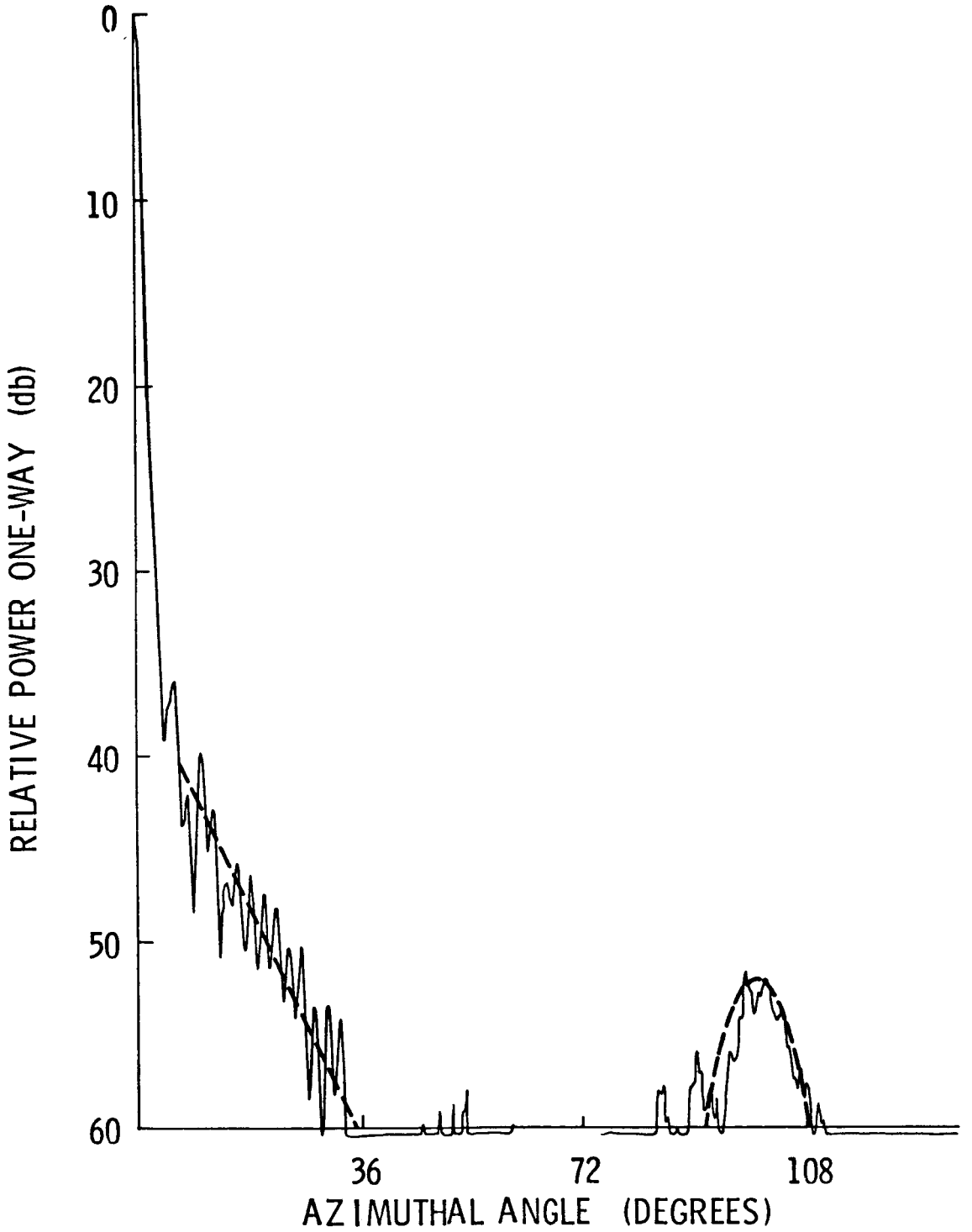

FIGURE 6. H PLANE PATTERN AT 13.9 GHz FOR THE AAFE RADSCAT ANTENNA

The cross polarized pattern was primarily significant in a vicinity about boresight. The relative phase β_p between polarizations was not available during these simulation studies. Fortunately for this antenna, the factors in the inversion model involving β_p may be regarded as negligible since the cross polarized pattern was localized about the boresight site axis and its maximum intensity was more than 20 dB beneath the polarized pattern. This implies $\sqrt{g_{p1} g_{p2}} \sin 2\Psi$ is insignificant in comparison to other terms in the vicinity of the boresight axis. (However, for another antenna this factor may be significant). The pattern representations should be considered expedient ones which are adequate to evaluate the inversion model rather than accurately specifying the actual patterns. The major effects have been preserved however.

The pattern representations together with the polarization mis-match factors $\cos^2\Psi$ and $\sin^2\Psi$ were employed to evaluate numerically the elements a_{kj}, b_{kj}, c_{kj}, and d_{kj} in the model. Numerical integrations over the spherical bands Ω_j were performed with Gaussian-Legendre quadrature techniques [16]. The numerical integrations roughly require the same amount of computer time regardless of the number of observation points $\{\theta_k: k = 1,2,\ldots,n\}$ since it is governed primarily by the antenna pattern sampling requirement of the quadrature method. Numerical integration in two or more dimensions typically consumes large amounts of computer time and, in this instance, since a transformation is required between the domain of integration and the pattern coordinates, the time is substantially larger.

The relative antenna weighting factors on 5° bands for a measurement at an observation angle (θ_o) of 40° on the v port are illustrated in the graphs of Figure 7. The solid line, plotted from the A matrix, represents the antenna sensitivity to the vertically polarized emissions; whereas the dashed line, plotted from the B matrix, represents the antenna sensitivity to the horizontally polarized emissions. The graphs demonstrate that the antenna temperature will be composed of contributions from both surface polarizations virtually over the whole space with the primary part coming from the main beam. Although no band off the main beam contributes significantly when considered alone, the total contribution from all these bands can be significant (even for this reasonably efficient antenna). The largest weight on the horizontally polarized emission (nearly 1%) is largely attributable to the cross polarized pattern. On the otherhand, the remaining horizontally polarized

weights are entirely a result of cross coupling ($g_{v1} \sin^2\psi$) between the polarized pattern and the "cross" polarized surface emission since the cross polarized pattern vanished outside the immediate vicinity of the main beam. From the graphs of Figure 7 it is observed that this cross coupling effect is comparable with the like coupling effect for contributions entering off the main beam.

A 38 x 38 modeling matrix representing 19 sample points at 10° intervals and both polarization were prepared. However, the inversions for the apparent temperatures were actually performed with a 38 x 28 matrix which resulted from considering the apparent temperature polarization invariant above the horizon and at nadir.

C. Computed Antenna Temperature Characteristics

The antenna temperatures at 10 degree intervals were accurately computed for temperature distributions typifying the emission characteristic over the sea as observed at 7 kilometers for two sky conditions. The distributions for the two sky conditions are shown in the graphs of Figures 8 and 9 and are based on the efforts of Wu [17] and Wu and Fung [18]. The differences between the antenna temperatures and actual polarized temperature distributions are shown in Figures 10 and 11. It is readily apparent that the antenna temperature is a crude measure of the actual temperature distribution. The deviation from the apparent temperature is typically largest at 90 degrees. Comparative studies of the polarized antenna temperatures would be sensitive to the different error characteristics as demonstrated by the graphs.

D. Estimating the Apparent Temperature

The above simulated antenna temperatures were used in the rectangular inversion model described above. The least squares solutions yielded estimates of the apparent temperatures for both sky conditions. The differences between the computed and actual temperatures are shown in Figures 12 through 15 for the two sky conditions and two polarizations. From these graphs it is apparent that better than an order of magnitude of improvement over that provided by the antenna temperatures can be realized for most look angles. The error in the temperature estimates for $\theta_o > 140^\circ$ are not shown in the graphs since the errors were negligible. In contrast to the antenna temperature error characteristics, the computed apparent temperature errors are largely independent of polarizations and the actual distributions. It is anticipated that the errors near the horizon could be reduced by sampling there more often.

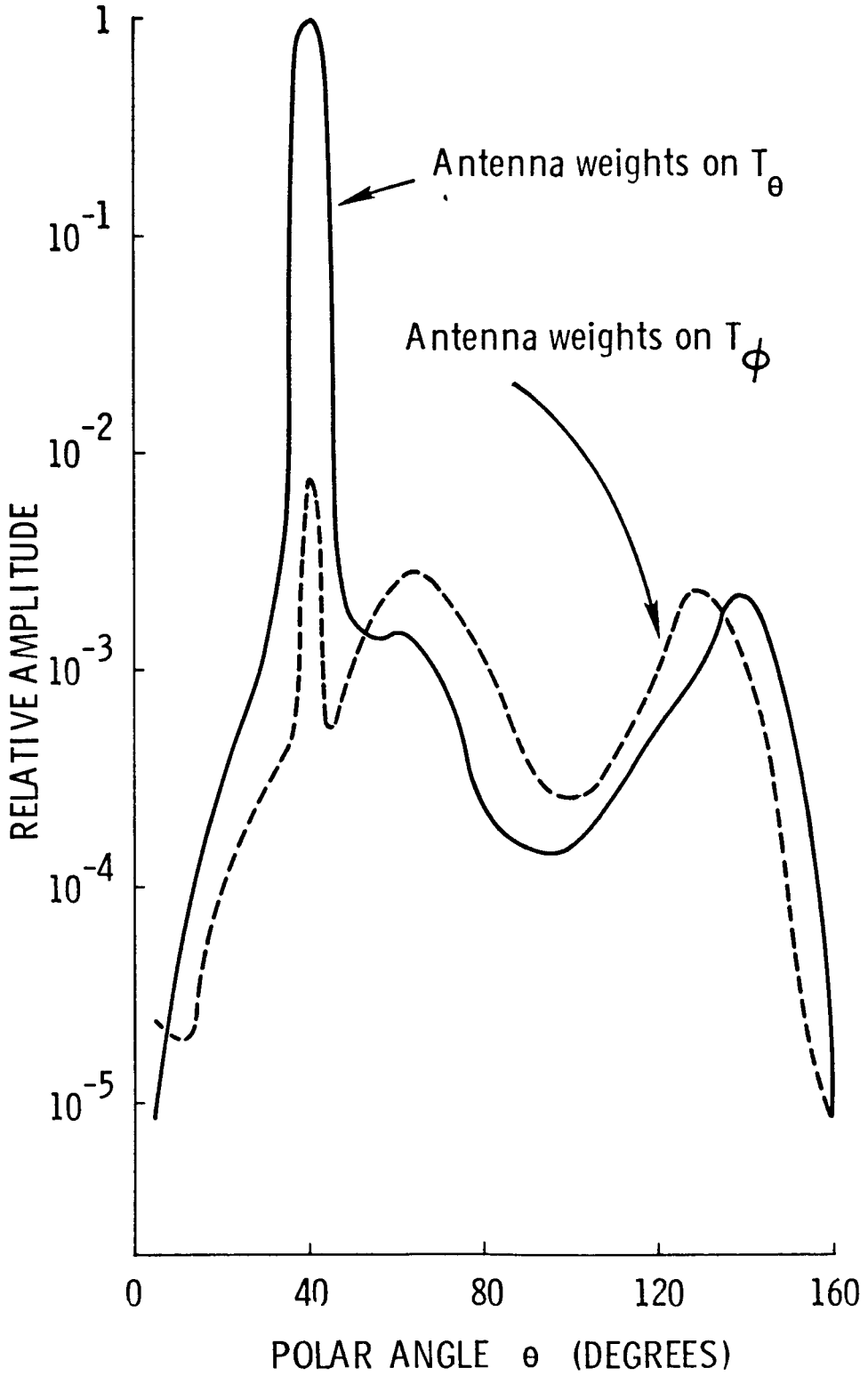

FIGURE 7. MODEL WEIGHTING FACTORS AS A FUNCTION OF POLAR ANGLE FOR A VERTICALLY POLARIZED OBSERVATION AT 40 DEGREES

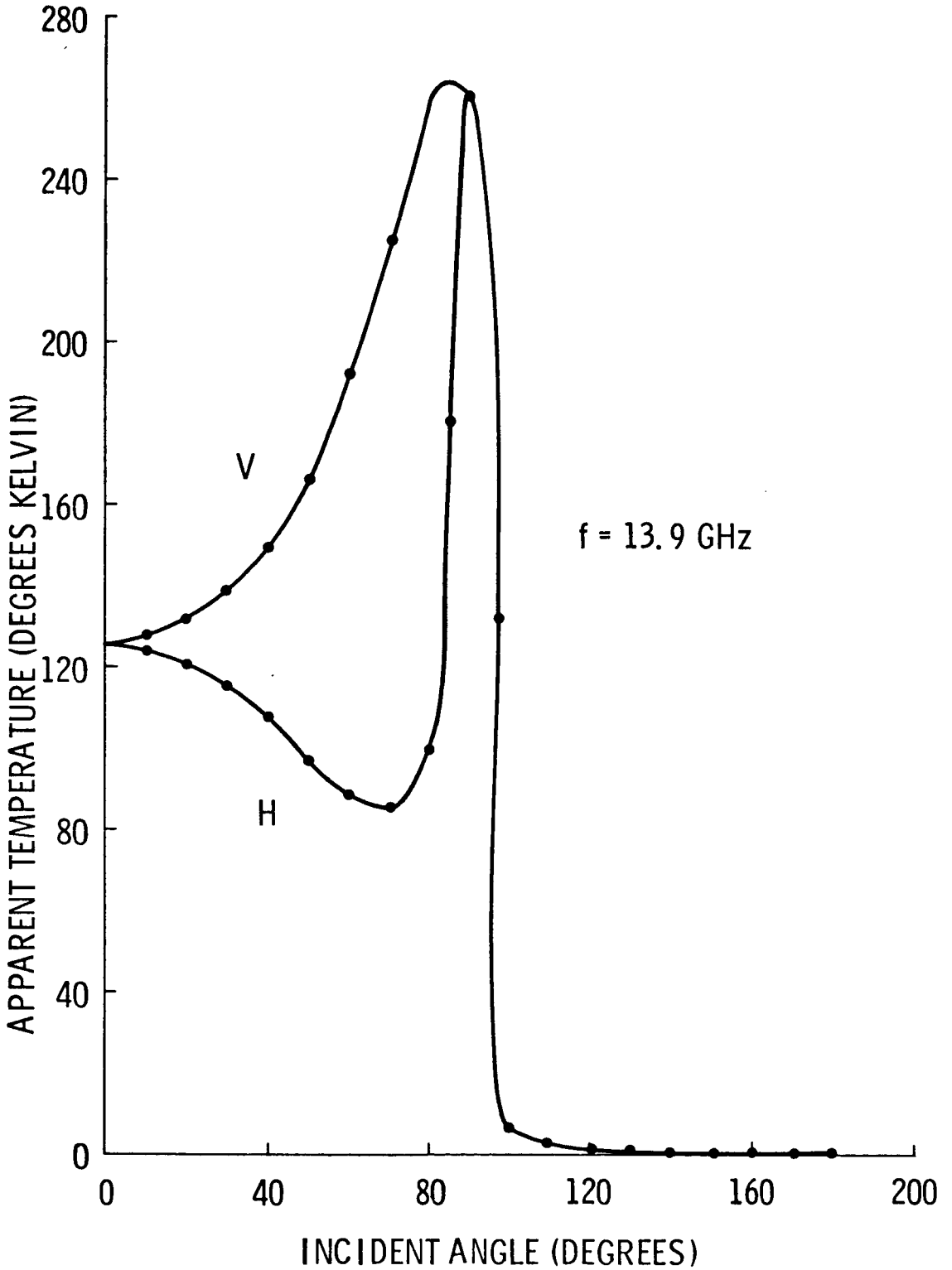

FIGURE 8. TEMPERATURE DISTRIBUTIONS SIMULATING CLEAR SKYS OVER THE OCEAN AS OBSERVED AT AN ALTITUDE OF 7 KILOMETERS

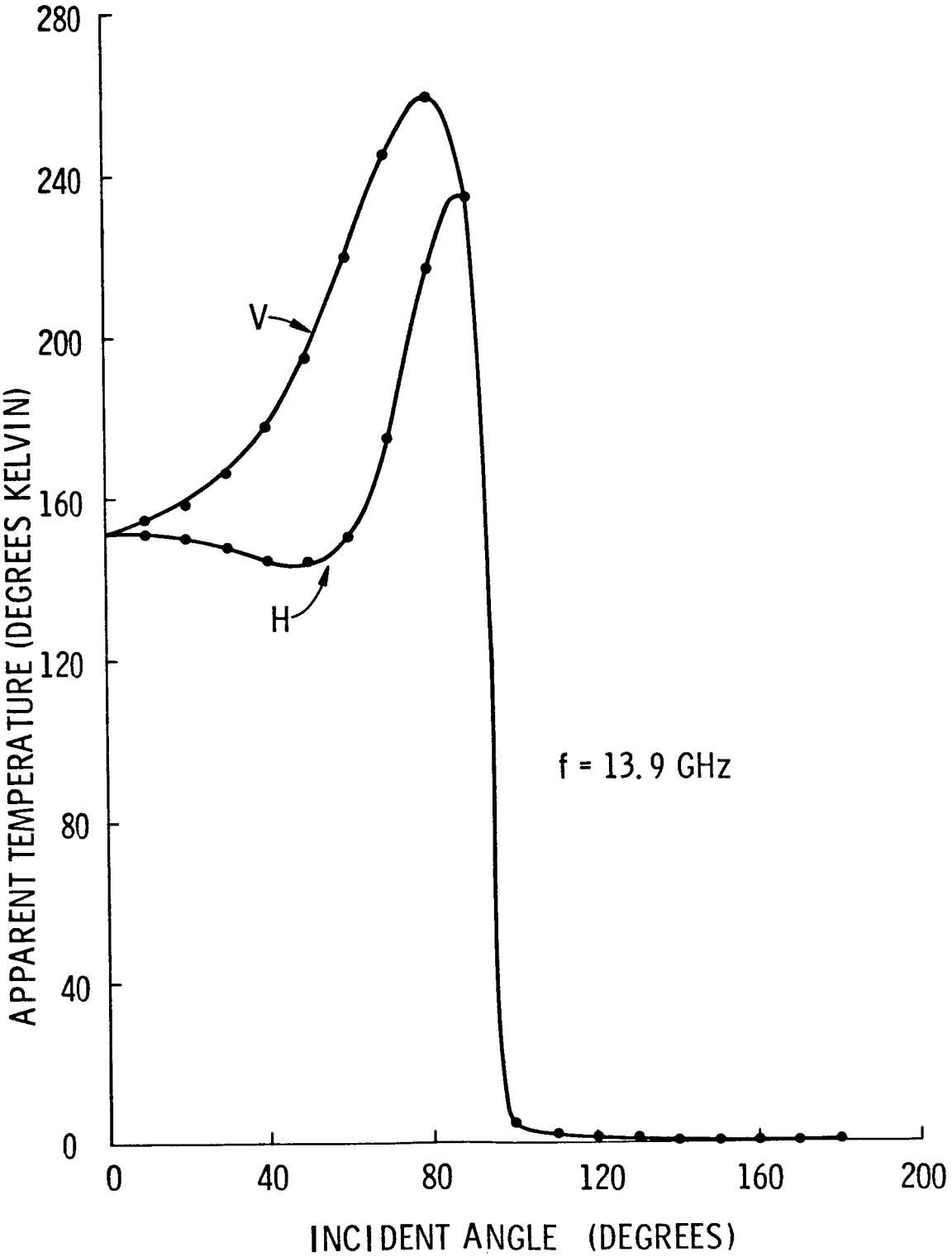

FIGURE 9. TEMPERATURE DISTRIBUTIONS SIMULATING HEAVY OVERCAST CONDITIONS OVER THE OCEAN AS OBSERVED AT AN ALTITUDE OF 7 KILOMETERS

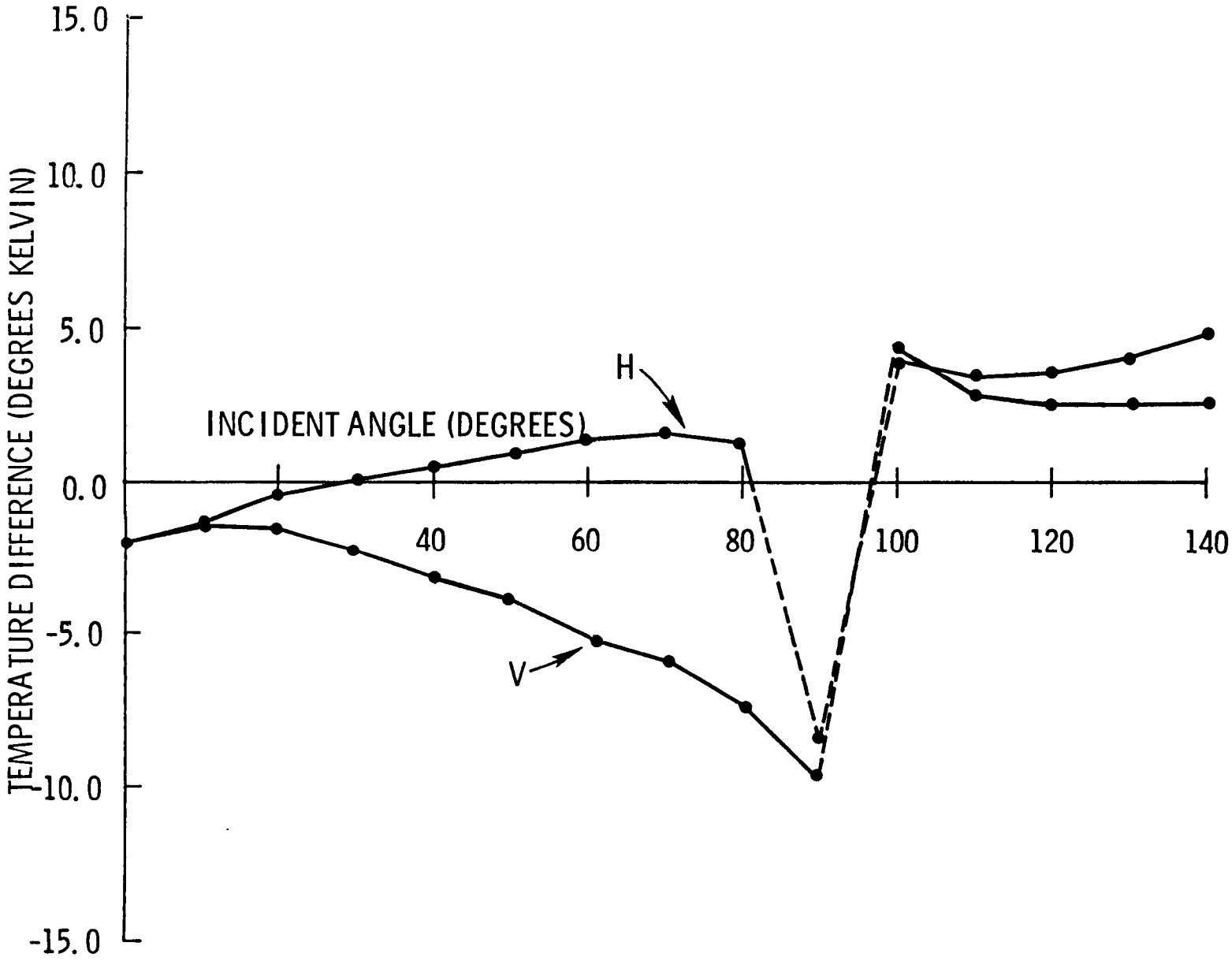

FIGURE 10. COMPARISON OF THE ANTENNA TEMPERATURE WITH THE RESPECTIVE POLARIZED TEMPERATURE DISTRIBUTION FOR THE CLEAR SKY CASE.

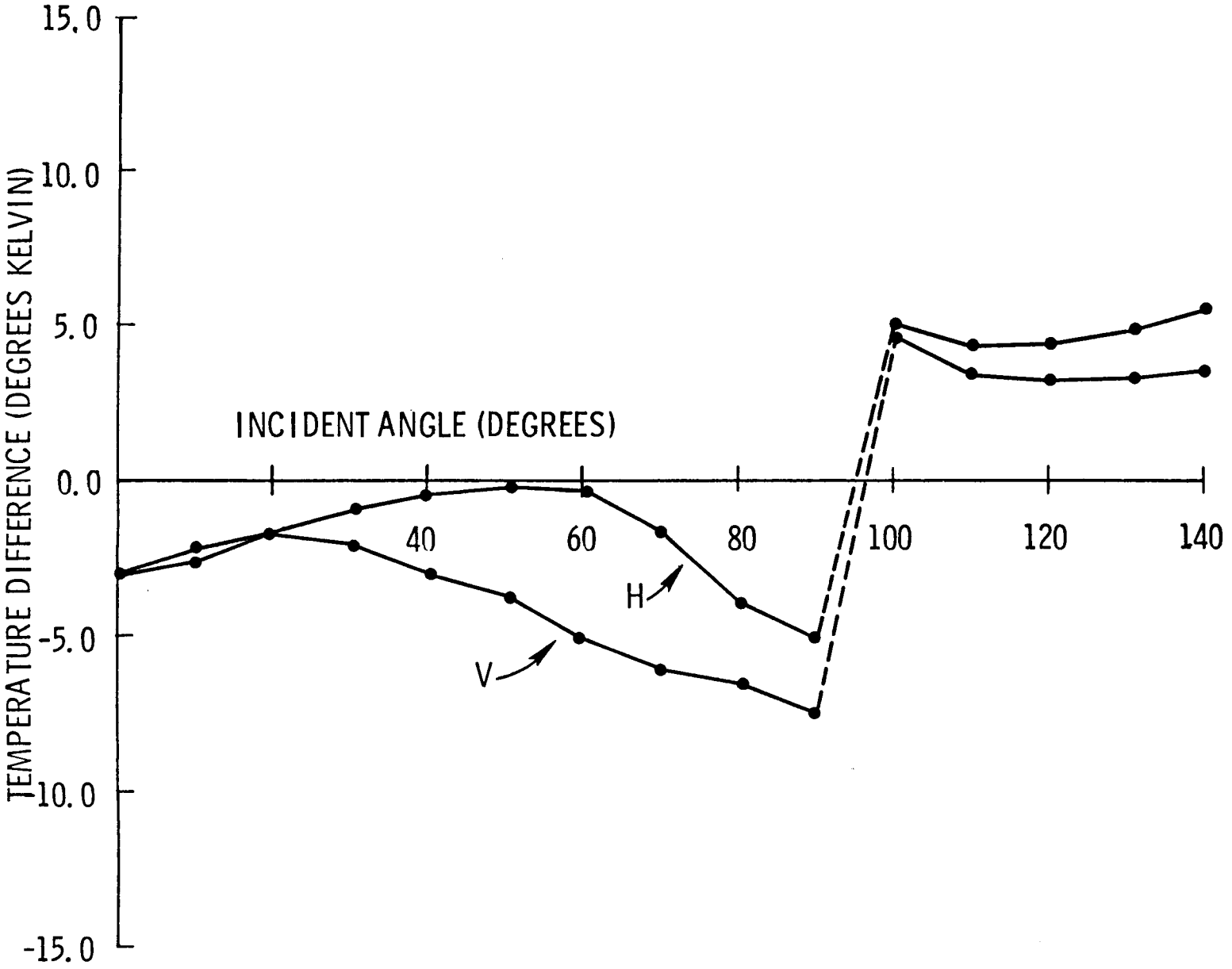

FIGURE 11. COMPARISON OF THE ANTENNA TEMPERATURE WITH THE RESPECTIVE POLARIZED TEMPERATURE DISTRIBUTION FOR THE OVERCAST CASE.

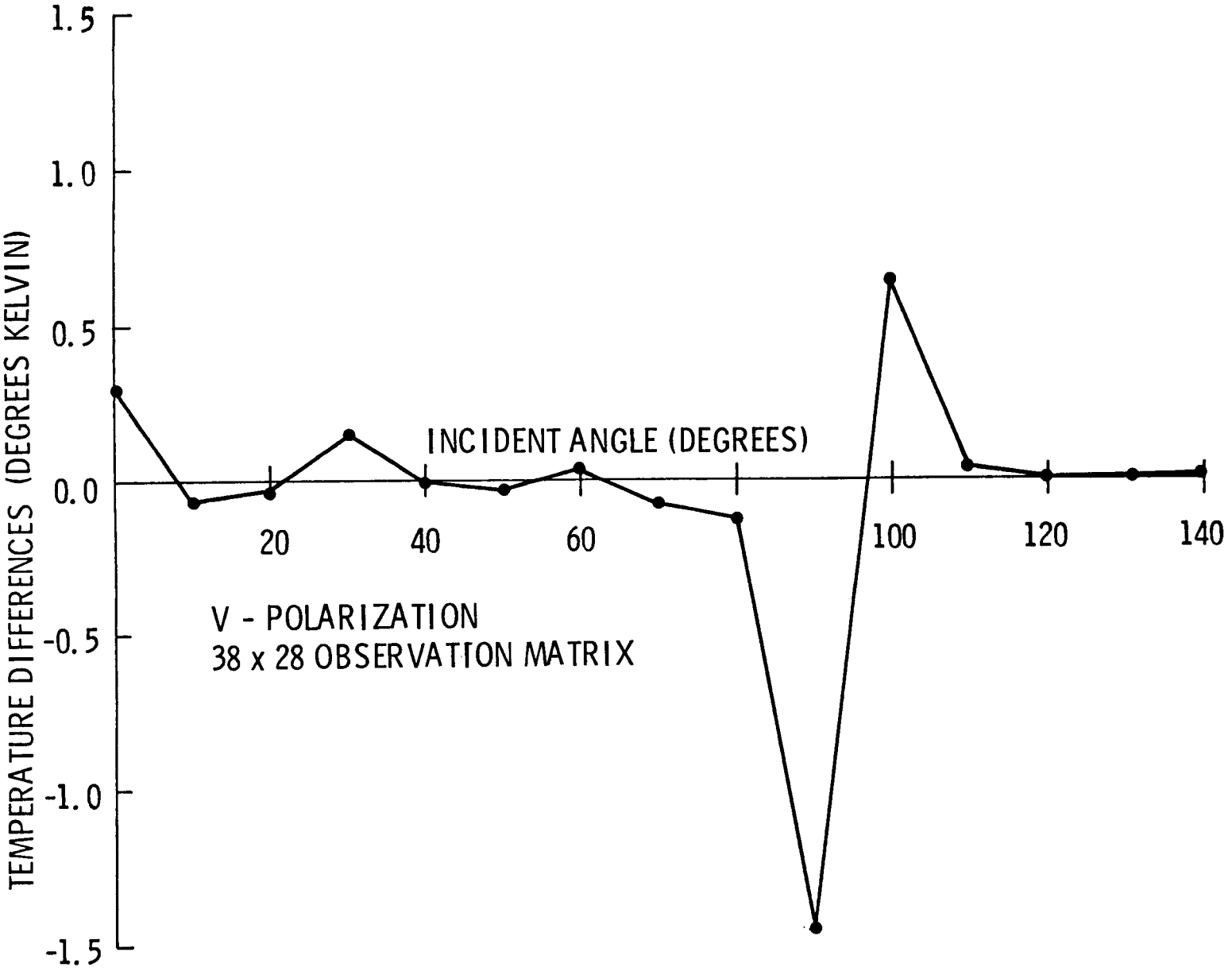

FIGURE 12. COMPARISON OF COMPUTED AND ACTUAL APPARENT TEMPERATURE FOR CLEAR SKY CASE.

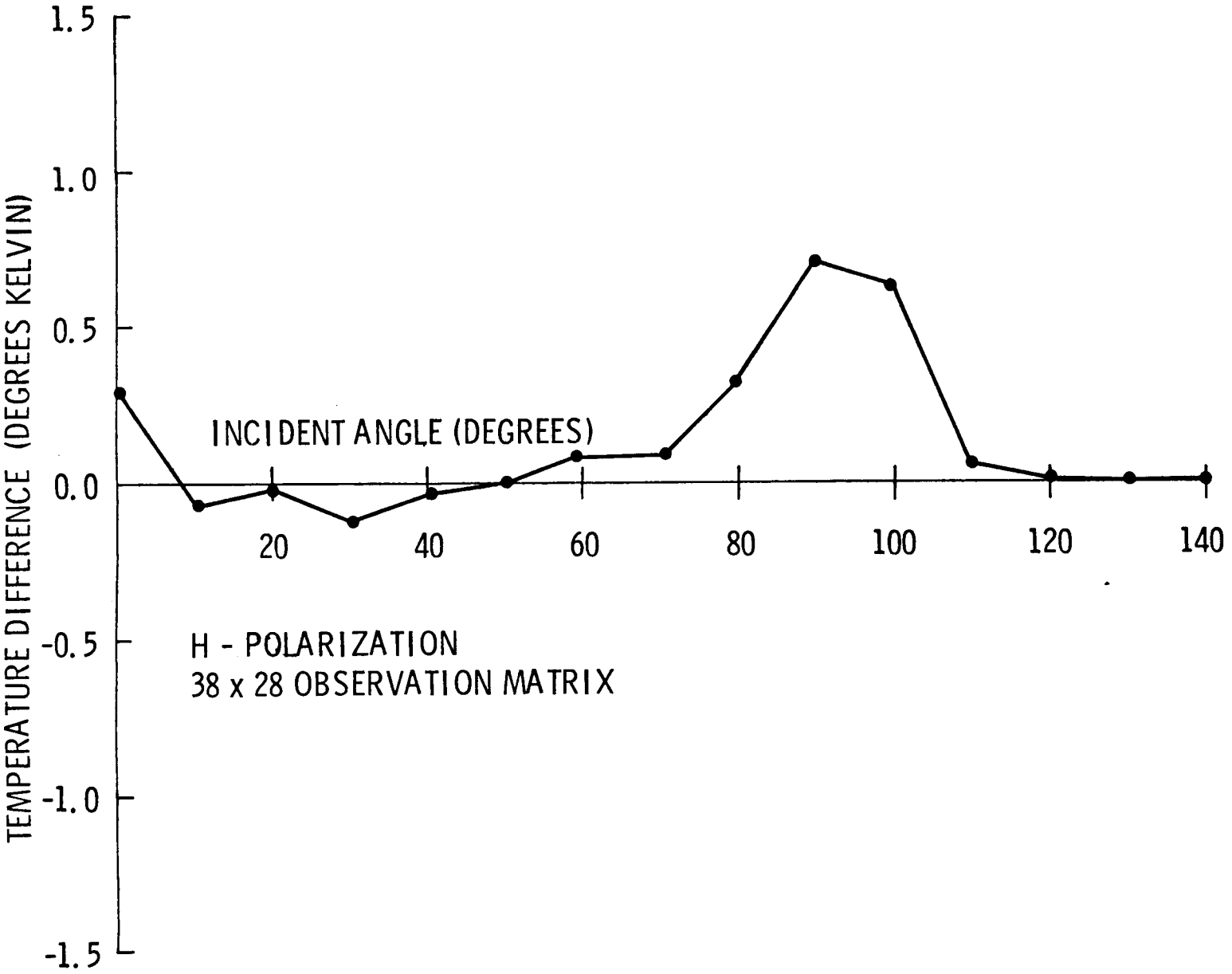

FIGURE 13. COMPARISON OF COMPUTED AND ACTUAL APPARENT TEMPERATURE FOR CLEAR SKY CASE.

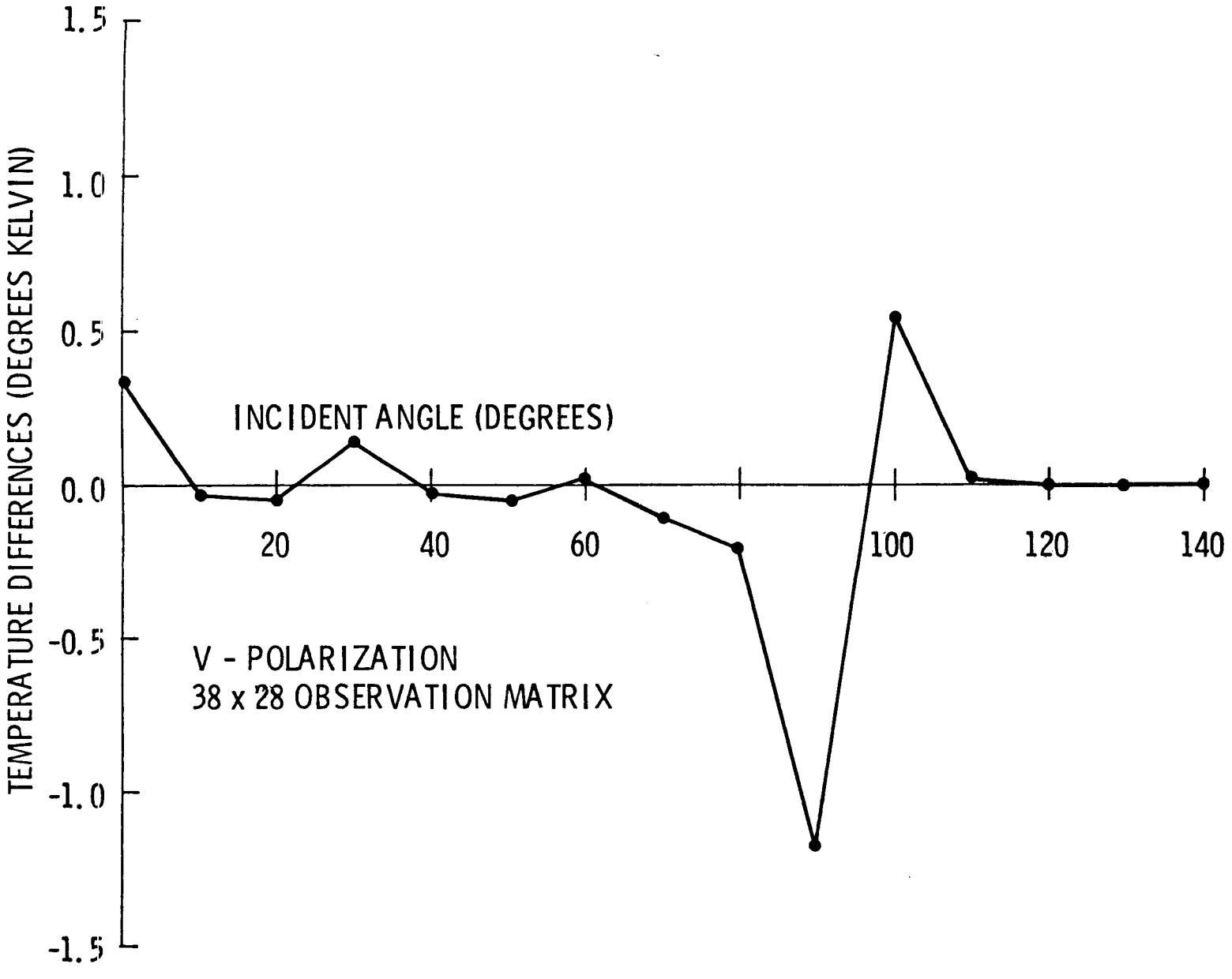

FIGURE 14. COMPARISON OF COMPUTED AND ACTUAL APPARENT TEMPERATURES FOR OVERCAST SKY CONDITION.

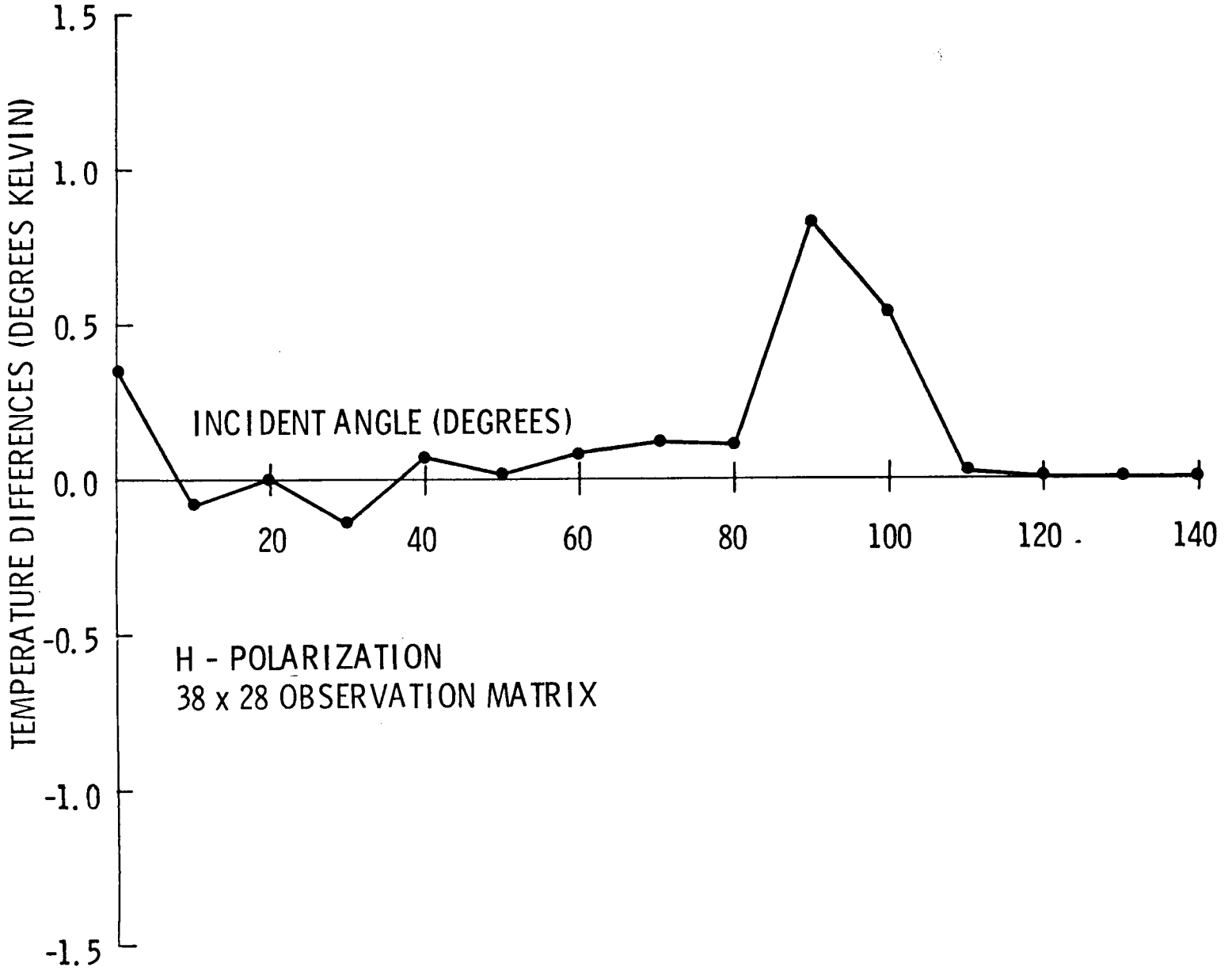

FIGURE 15. COMPARISON OF COMPUTED AND ACTUAL APPARENT TEMPERATURES FOR OVERCAST SKY CONDITION.

CONCLUSIONS AND COMMENTS

An integral inversion method based on a matrix approximation of the integral has been successfully applied to yield good estimates of the apparent temperature distributions from simulated antenna temperatures. These results have shown that cross coupling between antenna polarizations and surface polarizations contributes significantly to the antenna temperature. Any inversion method for scenes having a polarized character must, as a consequence, account for contributions from both emitted polarizations. To adequately discern the polarization effects in the inversion model, comprehensive knowledge of the polarized and cross-polarized antenna patterns are also required to compute the entries in the observation matrix. In view of the cross-coupling and the existence of cross polarized patterns, it is necessary that measurements be conducted at both polarizations to realize a thorough inversion.

The sensitivity of the above model to errors in the observation vector $\begin{bmatrix} Tv \\ Tn \end{bmatrix}$ or in the modeling matrix were not considered above. The reader may astutely question the behavior of the solution technique in the presence of errors. Some preliminary results have indicated that the errors in the estimate follow the error character inserted in the observation vector. The dominant diagonal of the modeling matrix would lead one to expect this result. Numerical filtering [12] reduced the error sensitivity slightly. Sensitivities in the modeling matrix have not yet been examined.

Although the preparation of the inversion model represents a sizeable computer effort (in addition to the measurement of the patterns), once the model has been prepared, it may be rapidly and repeatedly applied to observations from many scenes which have been sampled at the same intervals. The method, in this respect, is efficient for large volumes of data, when compared to iterative or Fourier transform methods where integrations are required repeatedly for each scene.

These simulation studies and studies performed by Peake et al. [1] have demonstrated that antenna temperatures serve as a crude and sometimes poor measure of the actual temperature distribution. The problem is particularly acute when side, spill-over, and back lobes make significant contributions to the antenna temperature. Thus precision radiometry, in the sense of recovering the apparent temperature distributions, involves more than precision at the antenna terminals. Unless highly efficient, narrow-beam antennas having low cross-polarized patterns are employed, compensation for antenna pattern weighting effects is clearly a prerequisite for exacting studies of microwave emission characteristics.

REFERENCES

[1] Peake, W. H., R. L. Riegler and C. H. Schultz, "The Mutual Interpretation of Active and Passive Microwave Sensor Outputs", Proceedings of the Fourth Symposium on Remote Sensing of Environment, University of Michigan, pp. 771-777, April, 1966.

[2] Bracewell, R. N., and J. A. Roberts, "Aerial Smoothing in Radio Astronomy" Australian Journal of Physics, Vol. 7, No. 4, pp. 615-640, Dec. 1954.

[3] Bracewell, R. N., "Interferometry and the Spectral Sensitivity Island Diagran," IRE Trans. on Antenna and Propagation, Vol AP-9, pp 59-67, Jan. 1961.

[4] Ryle, M. and D. D. Vonberg, "An Investigation of Radio Frequency Radiation from the Sun", Proceeding of the Royal Society, Vol. 193A, pp 98-120, April 1948.

[5] Bracewell, R. N., "Correcting for Gaussian Aerial Smoothing", Australian Journal of Physics. Vol. 8, No. 1, pp. 54-59, March, 1955.

[6] Hidy, G. M., W. F. Hall, W. N. Hardy, W. W. Ho, et al., Development of a Satellite Microwave Radiometer to Sense the Surface Temperature of the World Oceans, North American Rockwell Corp., NASA CR-1960, 1972.

[7] Tricomi, F. G., Integral Equations, Interscience Publishers, Inc., New York, p 6, 1970.

[8] Bracewell, R. N., Restoration in the Presence of Errors, Proceedings of the IRE, Vol. 46, No. 1, pp 106-111, Jan. 1958.

[9] Westwater, E. R. and O. N., Strand, "Inversion Techniques," in Remote Sensing of the Troposphere, V. E. Derr (Editor), NOAA, U. S. Department of Commerce, U. S. Printing Office, Washington, D. C., August 1972.

[10] Ko, H. C., "Coherence Theory of Radio-Astronomical Measurements", IEEE Transaction on Antennas and Propagation, Vo. AP-15, No. 1 pp 10-20, Jan. 1967.

[11] Aoki, Masanao, Introduction to Optimization Techniques, The Macmillan Company, New York, pp. 29-35, 1971.

[12] Twomey, S., "The Application of Numerical Filtering to the Solution of Integral Equations Encountered in Indirect Sensing Measurements", Journal of the Franklin Institute, Vol. 279, No. 2, February, 1965.

[13] Born, M. and E. Wolf, Principles of Optics, Pergamon Press, Chapter 10, 1959.

[14] Kales, M. L., Elliptical Polarized Waves and Antennas, Part III, Proceedings of the IRE, Vol. 39, No. 5, pp. 544-549, May, 1951.

[15] Ko, H. C., "Antenna Temperature and the Temperature of Electromagnetic Radiation", IEEE Transaction on Antennas and Propagation, Vol. 12, No. 1, pp. 126-127, Jan 1964.

[16] Klerer, M. and G. A. Korn, Digital Computer User's Handbook, McGraw-Hill, p. 2-130, 1970.

[17] Wu, S., "The Meteorological Effects on Microwave Apparent Temperatures Looking Downward Over a Smooth Sea", University of Kansas Center for Research, Technical Report 186-1, October, 1970.

[18] Wu, S. T. and A. K. Fung, "A Noncoherent Model for Microwave Emissions and Backscattering from the Sea Surface", Journal of Geophysical Research, Vol. 77, No. 30, pp. 5917-5929, October 20, 1972.